Classification of movement intention by spatially filtered electromagnetic inverse solutions

Marco Congedo, Fabien Lotte, Anatole Lécuyer

Classification of movement intention by spatially filtered electromagnetic inverse solutions

ACCEPTED FOR PUBLICATION FEB 2006 IN "PHYSICS IN MEDICINE AND BIOLOGY". AUTHORS' DRAFT

M. Congedo[1-3], **F. Lotte**[2] **and A. Lécuyer**[2]
1 France Telecom R&D, Tech/ONE Laboratory, 28 Chemin du vieux Chêne, InoVallée, 38240, Grenoble, France.
2 French National Institute for Research in Informatics and Random Systems (IRISA), Campus de Beaulieu. F - 35 042 Rennes Cedex, France.

Abstract. We couple the standardized low-resolution electromagnetic tomography (sLORETA), an inverse solution for electroencephalography (EEG) and the common spatial pattern, which is here conceived as a data-driven beamformer, to classify the benchmark BCI (Brain Computer Interface) competition 2003, data set IV. The data-set is from an experiment where a subject performed a self-paced left and right finger tapping task. Available for analysis are 314 training trials whereas 100 unlabeled test trials have to be classified. The EEG data from 28 electrodes comprise the recording of the 500 ms before the actual finger movements, hence represents uniquely the left and right finger movement intention. Despite our use of an untrained classifier, and we extract only one attribute per class, our method yields accuracy similar to the winners of the competition for this data-set. The distinct advantages of the approach presented here are the use of an untrained classifier and the processing speed, which make the method suitable for actual BCI applications. The proposed method is favourable over existing classification methods based on EEG inverse solution, which either rely on iterative algorithms for single-trial independent component analysis or on trained classifiers.

Keywords. Brain Computer Interface, Movement Intention, Beamforming, Joint Diagonalization, EEG, Inverse Solution, sLORETA, Common Spatial Pattern, Permutation Tests.

1. Introduction

By means of a Brain Computer Interface (BCI) humans can send simple commands to electronic devices without using motor activity. A major line of research pursues this goal by the acquisition of volitional control over the production of specific brain activities (Kübler *et al*, 2001; Wolpaw *et al*, 2002). A typical example is the imagination of limb movement, which engenders negative potentials (Bereitschaft Potential) and desynchronization of mu and beta oscillatory activity (Movement Event-Related Desynchronisation) in the contralateral primary motor cortex. The extraction and classification of these brain activities as belonging to left or right limb movement intention enables the emission of a binary command (Blankertz *et al*, 2002; Müller *et al*, 2004; Pfurstcheller *et al*, 1993; Wang *et al*, 2004). This bit of information may be coded arbitrarily, e.g., for displacing a cursor on the screen, opening/closing a hand orthosis, or spelling text. BCI systems have been originally conceived to provide a means of communication to people affected by "locked-in" syndrome. As a consequence of amyotrophic lateral sclerosis, brainstem stroke, brain or spinal cord injury, multiple sclerosis and several other diseases, human beings may experience difficulties in communicating with the external world. For the most severe impairments, a BCI offers the only possible channel of communication, thus it represents the only way for improving the quality of life of the patient (Neumann *et al*, 2003). Currently, the potential of BCI as an alternative or additional interface modality has been widely recognized and research is in progress linking BCI to new applications in multimedia technology.

Traditionally, a great deal of attention has been devoted to the accuracy of the classification algorithm. For most existing BCI systems a long learning phase based on many training trials is necessary. Besides the characteristics of the method itself, the accuracy of the classification depends on at least three factors, namely, the measurement's signal-to-noise ratio (SNR), the degree

[3] Corresponding Author. Telephone: +33 4 76764339. E-mail: Marco.Congedo@gMail.com

of distinction of the extracted attributes and the simplicity of the brain feature under consideration[4]. Several forms of cerebral and extra-cerebral noise mask the membership and are a major cause of misclassification. On the other hand, how well the extracted attributes are distinct and separable depends strictly on how they are defined and processed, i.e., how specifically and precisely each attribute independently represents the different intentions of the user. The third confounding factor is the fact that the brain does not seem to reproduce one-to-one relationships between mental and physiological states. In general, the more elementary the brain process, the lower the inter-individual and intra-individual variability, yielding a more consistent brain feature to be extracted for classification purposes.

The aim of this paper is to introduce, formalize and evaluate the conjunction of data-driven spatial filters and electromagnetic source localization for the extraction of separable attributes related to left and right finger movement intention. The method is non-invasive and has only one major requirement; that the observable brain activities associated with each command are generated by sources with *different spatial location* in the neocortical volume. If this is the case, as for the desynchronization engendered by limb movement intention, it seems a natural choice to derive the relevant attributes taking advantage of the spatial segregation of their sources. This may be accomplished by, and is the very aim of, source localization methods (for a review see Michel *et al*, 2004). Little work has been done investigating this opportunity, probably because several limitations of the EEG (electroencephalography) inverse problem need to be appropriately addressed for such an approach to be effective. Qin *et al* (2004) successfully combined independent component analysis (ICA), a data-driven method to solve the blind source separation (BSS) problem (Cichocki and Amari, 2002, Hyvärinen, *et al*, 2001), and frequency-specific cortical current density projection to classify a motor imagery dataset without training. Jun *et al* (2005) proposed to combine ICA and a source localization method based on a multi layer neural network with the same goal. Grave de Peralta Menendez *et al* (2005) reported high classification accuracy using a trained classifier based on frequency-domain inverse solution.

In this paper sLORETA, the standardized low-resolution electromagnetic tomography (Pascual-Marqui, 2002), is used to detect activity of the left and right motor cortex using only 28 EEG channels and an untrained classifier. sLORETA is a data-independent minimum norm inverse method featuring exact localization of single sources (Greenblatt *et al*, 2005; Pascual-Marqui, 2002, Sekihara *et al*, 2005). It is known to suffer from poor spatial resolution and to be negatively affected by noise. Both limitations add on as confounding factors and in general sLORETA alone does not allow satisfactory classification accuracy. This is shown in the Results section. Therefore, a spatial filter is introduced to enhance the left/right segregation capability of the sLORETA reconstruction, reducing the negative effect of both noise and poor spatial resolution. As compared to previous works our approach is a hybrid, in the sense that the classifier is untrained but some learning is required to find the suitable spatial filter. Thus, while our method adapts to the individual characteristics, it also allows fast classification, which stems from the fact that it does not require the lengthy iterative computations needed for the extraction of relevant components by ICA. More importantly, our method does not need an algorithm for the real-time automatic selection of relevant independent components for each trial, a task that so far has proven elusive.

In section 2 we present a suitable theoretical framework to obtain spatially filtered sLORETA estimations based on inverse quadratic form operators. In section 3 we show that the common spatial pattern (CSP), a spatial filter previously employed for classification purposes (Blanchard and Blankertz, 2004; Guger *et al*, 2000; Ramoser *et al*, 2000), is optimal for maximizing the separation of sLORETA source power associated with the left and right hand movement intention as observed in the involved sectors of the primary motor cortex. The filter is here derived within a functional optimization framework, following the literature on beamforming (Van Veen and Buckley, 1988). A connection with the BSS problem is suggested as well. The performance of the method is assessed on self-paced left and right finger-tapping data from the BCI competition 2003,

[4] For the sake of terminological precision throughout this paper we will use the word *feature* to describe the brain activity of interest in general (motor cortex desynchronization), whereas by *attribute* we will refer to the specific extracted activity linked to each class (e.g., the left and right motor cortex desynchronization). Thus, for this study we consider one feature and we extracted two attributes.

data set IV (Blankertz *et al*, 2004). The description of the data-set, along with all details on the feature extraction/classification method and the results are reported in section 4. Although we extracted only one feature and rely on an untrained classifier, our method nearly reaches the accuracy of the winner of the BCI competition 2003 for this data-set, demonstrating not only the suitability of sLORETA for extracting brain activity related to movement intention, but also, that adequately defining the brain feature of interest may be as important as using multiple features and a trained classifier. Section 5 contains our conclusions and a discussion.

2. The inverse problem by quadratic forms

The *biomagnetic inverse problem* (Lopes da Silva, 2004; Sarvas, 1987) generally refers to the estimation of location and strength of the brain dipolar sources generating electric (or magnetic) activity detectable by extra-cranial sensor measurements. For any linear and discrete EEG inverse solution the estimation of the *source power* γ_Ω in a region of interest Ω (ROI) can always be expressed as a quadratic form reading

$$\gamma_\Omega(t) = \boldsymbol{v}^T(t)\boldsymbol{Q}_\Omega\boldsymbol{v}(t) = \left\|\boldsymbol{H}_\Omega^T\boldsymbol{v}(t)\right\|_2^2. \qquad (2.1)$$

In the first expression $\boldsymbol{v}(t)$ is a vector holding N instantaneous measurements at time sample t, superscript T denotes transposition and the matrix $\boldsymbol{Q}_\Omega$ is the quadratic inverse operator referred to as the *quadratic form matrix* for ROI Ω. In the second expression $\boldsymbol{H}_\Omega$ is obtained by full-rank factorization of $\boldsymbol{Q}_\Omega$, such that $\boldsymbol{H}_\Omega\boldsymbol{H}_\Omega^T=\boldsymbol{Q}_\Omega$ (see Appendix). $\|\cdot\|_2$ is the L2-norm. Whenever several time points are available, which is usually the case of real-time applications where a sliding window $\bar{t}$ of arbitrary length and ending at time instant t is recursively considered, γ_Ω can be estimated directly from the sensor average outer product matrix

$$\boldsymbol{V} = \left\langle \boldsymbol{v}(t)\boldsymbol{v}(t)^T \right\rangle. \qquad (2.2)$$

In (2.2) $\langle\cdot\rangle$ indicates averaging across the chosen time window. The estimation reads in this case

$$\gamma_\Omega(\bar{t}) = tr\left(\boldsymbol{H}_\Omega^T\boldsymbol{V}\boldsymbol{H}_\Omega\right), \qquad (2.3)$$

where $tr(\cdot)$ indicates the trace of a matrix.

To derive these results let us consider the *forward* problem, which consists in computing the observable surface potentials knowing location, orientation and strength of all current sources. After modelling of the physical characteristics of the propagation medium (head), the problem has an approximated analytical solution (Sarvas, 1987) given by linear equation

$$\boldsymbol{v}(t) = \boldsymbol{K}\boldsymbol{c}(t), \qquad (2.4)$$

where each one of the N-dimensional $3M$ columns of $\boldsymbol{K}$ holds the surface field (leadfield) for unit dipole basis component (x, y, z). Vector $\boldsymbol{c}(t)$ is $3M$-dimensional and holds the three dipolar current components for each one of M discrete voxels (volume element). Solving (2.4) for the current yields an undetermined system of equations admitting infinite solutions with form

$$\hat{\boldsymbol{c}}(t) = \boldsymbol{T}\boldsymbol{v}(t), \qquad (2.5)$$

where the transfer matrix $\boldsymbol{T}$ is a $3M{\cdot}N$ (right) generalized inverse of $\boldsymbol{K}$. The least squares (minimum norm) and Tikhonov regularized solution for common average referenced voltage is given in the EEG case by (Pascual-Marqui, 2002, Eq 11)

$$\boldsymbol{T} = \boldsymbol{K}^T\left(\boldsymbol{K}\boldsymbol{K}^T + \alpha\boldsymbol{X}\right)^+, \qquad (2.6)$$

where α is a non-negative regularization parameter taken as zero for noise-free measurements, $\boldsymbol{X}$ is the centering matrix (common average reference operator) and superscript + indicates Moore-Penrose pseudo-inverse. One detail should be noted here; (2.6) assumes that all columns of $\boldsymbol{K}$ are centered (common average of unit scalp fields), thus so must be the voltage measurements entering the inverse problem. That is to say, throughout this work we implicitly consider only EEG and leadfield referenced to the common average. Because of the referential nature of EEG the Gram matrix $\boldsymbol{K}\boldsymbol{K}^T$ (Gross and Ioannides, 1999) has N-1 non-null eigenvalues. Similarly, the signal subspace dimension of the sensor average outer product $\boldsymbol{V}$ (2.2) is at most N-1.

The minimum norm transfer matrix for α=0 is easily shown to be the Moore-Penrose pseudo-inverse of $\boldsymbol{K}$ and as such is unique. More precisely, it is the unique solution yielding both

minimum reconstruction error and minimum overall source power in the least-squares sense (Cichocki and Amari, 2002, p. 58). The resolution matrix (Backus and Gilbert, 1968; Pascual-Marqui, 1999a), sometimes called resolution kernel, $\boldsymbol{S}=\boldsymbol{TK}$, is far from the identity, from which the idea to obtain a standardization (sLORETA). In a Bayesian framework Pascual-Marqui (2002) shows that the resolution matrix is the actual source variance assuming the identity as its prior, $\boldsymbol{KK}^T+\alpha\boldsymbol{X}$ as the sensor variance prior and $\alpha\boldsymbol{X}$ as the noise variance prior. The standardized source power at voxel λ is then given by the author as

$$\gamma_\lambda(t)=\hat{\boldsymbol{c}}_\lambda^T(t)\boldsymbol{S}_\lambda^{-1}\hat{\boldsymbol{c}}_\lambda(t), \qquad (2.7)$$

where $\boldsymbol{S}_\lambda^{-1}$ is the inverse of the λ^{th} 3·3 diagonal block of the resolution matrix and $\hat{\boldsymbol{c}}_\lambda(t)$ is the λ^{th} triplet of (2.5). We see that the sLORETA source power is the square of the Mahalanobis distance of point $\hat{\boldsymbol{c}}_\lambda(t)$ from the origin. As a consequence, source power estimations all across the volume are expressed by sLORETA on the same dimensionless metric.

For our purpose let us express the source power estimation at voxel λ equivalently by means of quadratic form

$$\gamma_\lambda(t)=\boldsymbol{v}(t)^T\boldsymbol{Q}_\lambda\boldsymbol{v}(t), \qquad (2.8)$$

which is obtained substituting the right-hand side of (2.5) in (2.7) and posing

$$\boldsymbol{Q}_\lambda=\boldsymbol{T}_\lambda^T\boldsymbol{S}_\lambda^{-1}\boldsymbol{T}_\lambda. \qquad (2.9)$$

It is straightforward to see that for a ROI Ω composed of an arbitrary number of voxels $\lambda\in\Omega$ the total source power is simply obtained by setting

$$\boldsymbol{Q}_\Omega=\sum_{\lambda\in\Omega}\boldsymbol{Q}_\lambda, \qquad (2.10)$$

yielding the expressions (2.1) for time points and (2.3) for time windows. sLORETA is our choice as an inverse solution for this work, however everything we say henceforth applies to any linear inverse solution, for which $\boldsymbol{Q}_\lambda=\boldsymbol{T}_\lambda^T\boldsymbol{T}_\lambda$ and $\boldsymbol{T}_\lambda$ is found according to another method.

3. Spatial filters by joint diagonalization

Beamforming has been widely applied to systems of sensors and sources such as radar and sonar and have been lately adopted for directly solving the biomagnetic inverse problem (Greenblatt *et al*, 2005; Sekihara *et al*, 2005) or for improving the performance of other inverse solution methods (Bolton *et al*, 1999; Gross and Ionannides, 1999; Rodriguez *et al*, 2006). For our purposes, a spatial filter is sought to maximize the separation of source power estimation in two ROIs, while suppressing noise and interference of energy originating elsewhere in the brain. A spatial *filter* is here conceived as an $N{\cdot}D$ matrix $\boldsymbol{F}$ reducing the sensor space into the *beamspace* $\boldsymbol{F}^T\boldsymbol{v}(t)$. The beamspace has dimension $D<(N-1)$. The filtered source power estimation, after *projection*

$$\hat{\boldsymbol{v}}(t)=\boldsymbol{F}\boldsymbol{F}^T\boldsymbol{v}(t), \qquad (3.1)$$

yields expression formally identical to (2.1) and (2.3). That is to say, for a time point the filtered source power estimation reads

$$\hat{\gamma}_\Omega(t)=\hat{\boldsymbol{v}}(t)^T\boldsymbol{Q}_\Omega\hat{\boldsymbol{v}}(t)=\left\|\boldsymbol{H}_\Omega^T\hat{\boldsymbol{v}}\right\|_2^2, \qquad (3.2)$$

while for a time window reads

$$\hat{\gamma}_\Omega(\bar{t})=tr\left(\boldsymbol{H}_\Omega^T\hat{\boldsymbol{V}}\boldsymbol{H}_\Omega\right)=\sum_{h=1}^{H}\boldsymbol{h}_{\Omega h}^T\hat{\boldsymbol{V}}\boldsymbol{h}_{\Omega h}, \qquad (3.3)$$

where $\hat{\boldsymbol{V}}=\boldsymbol{F}\boldsymbol{F}^T\boldsymbol{V}\boldsymbol{F}\boldsymbol{F}^T$, H is the number of columns of full-column rank matrix $\boldsymbol{H}_\Omega$ (2.1) and $\boldsymbol{h}_{\Omega h}$ is its h^{th} column. The expressions for the filtered estimation as in (3.2) and (3.3) holds for both point regions (i.e., a single voxels) and extended regions (covering an arbitrary large volume), the only difference possibly being H. In the case of EEG, for point regions we have H=3, whereas for extended regions we have $H\geq3$.

The method we follow to derive the data-driven beamformers is the optimization of functional using extreme properties of eigenvalues (Bolton *et al*, 1999; Gross and Ioannides, 1999; Schott, 1997), which yields analytical solutions. Throughout this paper we will refer to L and R as to the ROI chosen to represent the sector of the left and right primary motor cortex implicated in the

desynchronization. Let $\boldsymbol{V}_{\mathrm{L}}$ and $\boldsymbol{V}_{\mathrm{R}}$ (2.2) be the grand average outer product of sensor measurements for available training trials corresponding to left and right limb movement intention, respectively. These two matrices, taken here as prototypes, carry a common covariance structure reflecting background noise plus interference (brain activity not related to the movement intention) and a peculiar covariance structure reflecting the source activity in L and R. The problem of extracting and maximizing the latter in L as compared to R and vice versa may be posed for each pair of vectors f_d and f_e of $\boldsymbol{F}$ such as

$$\max_{f_d}\left\{\frac{\boldsymbol{f}_d^T\boldsymbol{V}_L\boldsymbol{f}_d}{\boldsymbol{f}_d^T\left(\boldsymbol{V}_L+\boldsymbol{V}_R\right)\boldsymbol{f}_d}\right\},\ \max_{f_e}\left\{\frac{\boldsymbol{f}_e^T\boldsymbol{V}_R\boldsymbol{f}_e}{\boldsymbol{f}_e^T\left(\boldsymbol{V}_L+\boldsymbol{V}_R\right)\boldsymbol{f}_e}\right\}, \quad (3.4)$$

with constraint of unit norm for each vector of $\boldsymbol{F}$. Only N-1 vectors of $\boldsymbol{F}$ are considered because one degree of freedom is lost in the reference, as seen in section 2. A set of vector pairs maximally divergent in the sense of (3.4) is obtained by finding the $N{\cdot}N$-1 matrix $\boldsymbol{F}$ as the joint diagonalizer of $\boldsymbol{V}_{\mathrm{L}}$ and $\boldsymbol{V}_{\Sigma}=\boldsymbol{V}_{\mathrm{L}}+\boldsymbol{V}_{\mathrm{R}}$ (Fukunaga, 1990, p 33-34), i.e., in such a way to verify

$$\begin{cases}\boldsymbol{F}^T\boldsymbol{V}_{\Sigma}\boldsymbol{F}=\boldsymbol{I}\\ \boldsymbol{F}^T\boldsymbol{V}_L\boldsymbol{F}=\boldsymbol{W}\\ \boldsymbol{F}^T\boldsymbol{V}_R\boldsymbol{F}=\boldsymbol{I}-\boldsymbol{W}\end{cases} \quad (3.5)$$

where $\boldsymbol{W}$=diag($W_1\geq W_2\geq\ldots\geq W_{N\text{-}1}$), $\boldsymbol{I}$-$\boldsymbol{W}$=diag(1-$W_1\leq$1-$W_2\leq\ldots\leq$1-$W_{N\text{-}1}$). The vectors in $\boldsymbol{F}$ are sorted so to "absorb" progressively less and less energy from $\boldsymbol{V}_{\mathrm{L}}$ and more and more energy from $\boldsymbol{V}_{\mathrm{R}}$ and, by construction, the vectors f_1 and $f_{N\text{-}1}$ are those best differentiating the structural information embedded in those two matrices. Indeed the eigenvalues associated with those two vectors are the extrema attaining the maxima of the functionals in (3.4).

The matrix $\boldsymbol{F}$ actually holds all solutions to the first maximization problem in (3.4) and the same matrix, but with vectors in reverse order, holds the solutions to the second maximization problem. In other words, the two solutions are reflections to each other along the main diagonal. The *pairs* of corresponding vectors are f_1 and $f_{N\text{-}1}$, f_2 and $f_{N\text{-}2}$ etc.. For BCI purposes we will consider two filters $\boldsymbol{F}_{\mathrm{L}}$ and $\boldsymbol{F}_{\mathrm{R}}$, both of dimension $N{\cdot}D$, each one targeting the respective ROI and defined such that $\boldsymbol{F}_{\mathrm{L}}$ holds the first D<(N-1)/2 vectors of $\boldsymbol{F}$ while $\boldsymbol{F}_{\mathrm{R}}$ holds the last D<(N-1)/2 vectors of $\boldsymbol{F}$ in reverse order. To see how the filter acts let $\boldsymbol{F}=\left[\boldsymbol{F}_L\boldsymbol{N}\boldsymbol{F}_R\right]$ be an arbitrary partition of the joint diagonalizer, which number of vectors in each partition depends on the choice of D. Given the outer product matrix $\boldsymbol{V}_{test}$ of an unlabeled trial and since $\boldsymbol{F}\boldsymbol{F}^T=\boldsymbol{F}_L\boldsymbol{F}_L{}^T+\boldsymbol{N}\boldsymbol{N}^T+\boldsymbol{F}_R\boldsymbol{F}_R{}^T$, we can expand the filtered source power estimation for ROI L in (3.3), such as

$$\begin{aligned}&\hat{\gamma}_L=tr\left(\boldsymbol{H}_L^T\boldsymbol{F}\boldsymbol{F}^T\boldsymbol{V}_{test}\boldsymbol{F}\boldsymbol{F}^T\boldsymbol{H}_L\right)=\\ &tr\left(\boldsymbol{H}_L^T\boldsymbol{F}_L\boldsymbol{F}_L^T\boldsymbol{V}_{test}\boldsymbol{F}_L\boldsymbol{F}_L^T\boldsymbol{H}_L\right)+\ tr\left(\boldsymbol{H}_L^T\boldsymbol{N}\boldsymbol{N}^T\boldsymbol{V}_{test}\boldsymbol{N}\boldsymbol{N}^T\boldsymbol{H}_L\right)\ +\ tr\left(\boldsymbol{H}_L^T\boldsymbol{F}_R\boldsymbol{F}_R^T\boldsymbol{V}_{test}\boldsymbol{F}_R\boldsymbol{F}_R^T\boldsymbol{H}_L\right)+\\ &2tr\left(\boldsymbol{H}_L^T\boldsymbol{F}_L\boldsymbol{F}_L^T\boldsymbol{V}_{test}\boldsymbol{N}\boldsymbol{N}^T\boldsymbol{H}_L\right)+2tr\left(\boldsymbol{H}_L^T\boldsymbol{F}_L\boldsymbol{F}_L^T\boldsymbol{V}_{test}\boldsymbol{F}_R\boldsymbol{F}_R^T\boldsymbol{H}_L\right)+2tr\left(\boldsymbol{H}_L^T\boldsymbol{F}_R\boldsymbol{F}_R^T\boldsymbol{V}_{test}\boldsymbol{N}\boldsymbol{N}^T\boldsymbol{H}_L\right).\end{aligned} \quad (3.6)$$

By construction, the last three terms of the sum (cross-terms) vanishes as $\boldsymbol{V}_{test}$ approaches $\boldsymbol{V}_L$ or $\boldsymbol{V}_R$, that is, they are small for trials close to the prototypes. The first term, the projection on the *beamspace*, is maximized, while the third, which here we call the projection on the *antibeamspace*, is minimized. The second term describes an *indecision* region, the space spanned by the vectors of $\boldsymbol{F}$ which eigenvalues are similar, that is, the vectors creating a beamforming projection with minimal separation capability. The equivalent expression for $\hat{\gamma}_R$, the filtered source power estimation for ROI R, is obtained using $\boldsymbol{H}_{\mathrm{R}}$ instead of $\boldsymbol{H}_{\mathrm{L}}$ in (3.6); in this case the first term is minimized, while the third is maximized. Thus, the beamspace for one ROI is the antibeamspace for the other. Equation (3.6) shows the actual stop-band regions for filter $\boldsymbol{F}_{\mathrm{L}}$ and $\boldsymbol{F}_{\mathrm{R}}$. In conclusion, the two filtered source power estimations provide an ideal coupling of attributes for detecting separation of energy originating in two ROIs.

The derivation of a beamspace given by such filters associated to ROI L and R has been previously called *Common Spatial Pattern* (CSP). Several authors applied the CSP to EEG data for the purpose of extraction of abnormal EEG components (Koles, 1991), EEG source localization

(Koles and Soong, 1998) and for classification of trials for BCI feature extraction (Blanchard and Blankertz, 2004; Guger *et al*, 2000; Ramoser *et al*, 2000). However, none of the authors also applied the CSP to an inverse solution to target the *sources* of the scalp spatial patterns. We found this further step very effective for our purpose.

Another link to the literature is established considering that, under certain circumstances, the joint diagonalization of two covariance matrices has been shown to solve the blind source separation (BSS) problem (Parra and Seida, 2003). The problem, which is also the aim of independent component analysis (ICA), consists of estimating the time courses of the actual sources observing only a linear mixture of them. The problem is said to be blind because no knowledge of the mixing process, hence on the propagating medium, is assumed. In our case the observed mixtures are the sensor measurements (2.4) and the sources are the activities of neuronal clusters associated with each of two commands plus interference and noise. An advantage of considering the grand average outer product matrix is that inter-trial uncorrelated noise will asymptotically vanish in the averaging processing. However, noise correlated across trials, such as eye movements, which tend to have a similar temporal course, will not. It is well known that sources can be estimated by BSS methods only up to a trivial permutation (order) indeterminacy. We have already stated that the relevant sources are always found by the CSP to be associated with the first and last D vectors of the filter. The reason why this is the case here is evident from the construction of the filter (3.5).

4. Evaluation and method

In this section we report relevant information about the data set IV of the BCI competition 2003. This data set is used to evaluate the combination of inverse solution and data-driven spatial filters for extracting relevant brain features. We then detail the method of training data analysis, which consist in defining a suitable frequency band-pass region, an optimal spatial filter, and the two ROIs. Finally we set our classification criterion and report the results of the classification of the benchmark data.

4.1. The Data Set

The data set was recorded from a non-clinical subject during a self-paced key pressing task. The subject sat in a normal chair, with the arms relaxed on a table and fingers in the standard typing position at the computer keyboard. The task was to press with the index and little fingers keys using either the left or right hand, in a self-paced timing and self-chosen order. The experiment consisted of three sessions of six minutes each, with a few minutes of break between sessions. The average key pressing speed was one second. EEG was acquired at 28 leads (F3, F1, Fz, F2, F4, FC5, FC3, FC1, FCz, FC2, FC4, FC6, C5, C3, C1, Cz, C2, C4, C6, CP5, CP3, CP1, CPz, CP2, CP4, CP6, O1, O2) with a 1000 Hz sampling rate. The position of electrodes in realistic Talairach space (Talairach and Tournoux, 1988) according to the 3-shell spherical head model implemented in the freeware LORETA-Key (available for download at http: //www.unizh.ch/ keyinst/ NewLORETA/ LORETA01.htm) is shown in figure 1.

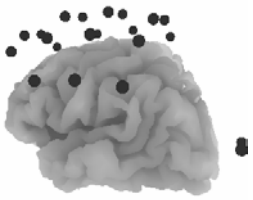

Figure 1. Electrode montage used to collect EEG in the BCI competition 2003, data set IV. The brain is seen from the left. All electrodes are depicted according to their actual position in the head model implemented in the LORETA-Key software as co-registered to the Talairach space.

Epochs of 500 ms were extracted ending 130 ms before the key press. The epochs were divided in a *training* set and a *test* set. There were 159 epochs for left movements and 157 epochs for right movements in the training set. The test set consisted of 49 epochs for left movements and 51 epochs

for right movement. Other details on the data-set can be found in Blankertz *et al* (2004). The task of the BCI competition 2003 for this data set was to classify the test trials using only the information contained in the training set.

4.2. Definition of Frequency Band-Pass Region

Our strategy for classifying these data is the spatial segregation of the contralateral desynchronization engendered in the motor cortex by the intention of movement of the left and right fingers. This activity is known to involve the frequency components mu and beta. The first step is then the definition of the frequency band-pass region better differentiating between the two alternative tasks. Before processing, we resampled the data to 128 samples per second by means of a natural cubic spline interpolation routine (Congedo *et al*, 2002). This sped up further computations and allowed the use of the fast Fourier transform algorithm, which requires power of two samples, without padding the data. The LORETA-Key software was used to compute the leadfield for a 3-shell spherical head model and for estimating the optimal amount of regularization for computing the sLORETA transfer matrix, that is, the α parameter in (2.6). For this purpose, all available training data entered a leave-one-out cross-validation procedure (Pascual-Marqui, 1999b). The regularization needed was estimated to be 10^4. The volume considered in LORETA-Key comprises 2394 voxels of dimension $7mm^3$ covering the gray matter according to the probability atlas of the Montreal Neurological Institute (Pascual-Marqui, 1999a). Next, we ran a sLORETA multiple comparison randomization-permutation *t*-max test (Holmes *et al*, 1996) in the frequency domain. The aim of the test is to compare voxel-by-voxel the mean source power in the left and right trials of the training set for sixteen 2-Hz frequency band-pass regions spanning the 2-32 Hz range. The test procedure repeatedly shuffles at random the labels "left" and "right" for training trials. At each shuffling (permutation), *t*-tests ("left" minus "right") are computed for all voxels to approximate the exact distribution of maximal *t*-statistics under the global null hypothesis (Holmes *et al*, 1996; Westfall and Young, 1993). Before entering the test procedure all source power values were natural log transformed and normalized to within-volume unit norm. The first transformation aims at approximating symmetry of spectral data, a weak assumption of the test, whereas the second minimizes the influence of artifacts and other abnormal activity with stronger energy than normal EEG. Notably, neither transformation alters the overall results of the test, but may help in preserving its power. What has been listed so far is standard statistical procedure for analyzing electromagnetic data in cognitive or clinical studies (for more details see Lubar *et al*, 2003. A freeware for multiple permutation tests is included in the NTE Pack 2005, available for download at www.NovaTechEEG.com). There are 2394 voxels for 32 frequency bins, for a total of 76608 simultaneous tests. The control of the family-wise error rate is guaranteed by the test procedure (Westfall and Young, 1993), i.e., the probability to erroneously reject even only one null hypothesis (declaring a voxel as significant whether it is not) is kept below 0.05. The test was run using 5000 random data permutations.

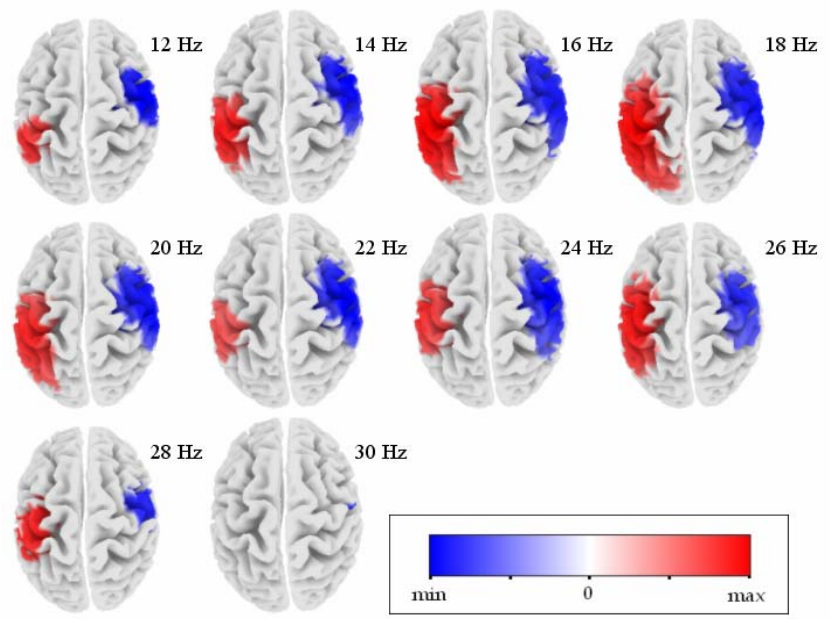

Figure 2: Significant results of the multiple-hypothesis permutation *t*-test comparing the mean source power of left and right training trials at each voxel. The cortical representation is the one implemented in the LORETA-Key software, which is based on the Atlas of Talairach and Tournoux (1988). All images are top views, with front of the brain up. Each image refers to the test for a frequency bin starting at 12 Hz and ending at 30 Hz, in 2-Hz increments. The voxel-by-voxel contrasts entered the test as left minus right, thus positive *t*-values (red-coded) indicate stochastic dominance of the source power produced by left movements trials while negative *t*-values (blue-coded) indicate stochastic dominance of the source power produced by right movements trials. Each image is scaled to its own absolute maximum. Only significant *t*-values (with family-wise error controlled at the 0.05 level) are colored.

The spatial distributions of the t-statistics for all frequency bins for which significant results were found are shown in the form of cortical images in figure 2. The threshold for rejecting the null hypothesis was found to be $t^*_{(312)}=\pm 4.33$, to which the corrected p-value upper bound of significance can be found by normal approximation to equal 0.00000745. Therefore these results depict *robust* shifts in the central tendency of the two distributions. Significant results were only found between 12 and 30 Hz. Evidently, as compared to right movement trials, left movement trials engender a desynchronization in the contralateral motor cortex and/or a synchronization of the ipsilateral motor cortex, and vice versa for right movement trials. Since data about a baseline (control) condition for each task is not available, that is all we can conclude with this test as far as hypothesis testing is concerned. However, from the literature, we know that intention of movement is associated with contralateral desynchronization rather than with ipsilateral synchronization. In any case, we are not concerned with the two marginal effects, but only with their interaction, as suggested in (3.5). Thus, for any practical purpose we can associate movement intentions with an increase in source power in the ipsilateral motor cortex. Qin *et al* (2004) arrived at this same conclusion.

Figure 3 shows the maximal and minimal *t*-statistic across the volume for each frequency bin and their relation with the threshold of significance. Refer to the caption for details. Following the graph, a sharp frequency window for which the central locations of the source power distribution in the two hemispheres maximally diverge is 14-26 Hz. All data (training and test) was therefore band-pass filtered using this range by means of inverse fast Fourier transform with a do-nothing (rectangular) time-domain tapering window.

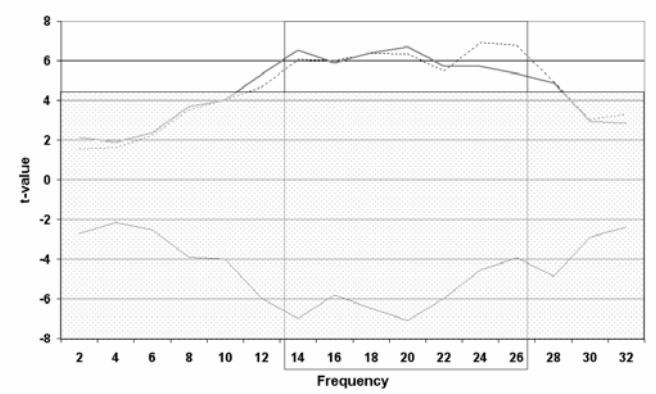

Figure 3. Frequency distribution of *t*-statistics maxima and minima in the volume. The lower dotted line plot indicates the (negative) *t*-minima, which are consistently found in the proximity of the right motor cortex. The upper dotted line plot indicates the (positive) *t*-maxima, which are consistently found in the proximity of the left motor cortex (see figure 2). The thick grey line plot in the upper portion of the graph is the average of the two extrema taken as absolute values. The semi-transparent panel in the foreground indicates the region of acceptance of null hypotheses as found by the permutation test. The vertical box includes the chosen frequency band-pass region.

4.3. Filter Definition

In this paper we use a single feature, the sLORETA filtered source power in two spatially segregated ROIs, L and R. The filter and the resulting projection of the data have been defined in (3.5) and (3.1), respectively. The projection aims at the maximal difference of the source power associated to each ROI. Using the 159 left fingers movement intention training trials and the 157 right fingers movement intention training trials we computed the grand average outer product sensor measurement matrices $\boldsymbol{V}_{\mathrm{L}}$ (left) and $\boldsymbol{V}_{\mathrm{R}}$ (right), already introduced in section 3. A method to find the joint diagonalizer $\boldsymbol{F}$ of matrices $\boldsymbol{V}_{\mathrm{R}}$ and $\boldsymbol{V}_{\Sigma}=\boldsymbol{V}_{\mathrm{R}}+\boldsymbol{V}_{\mathrm{R}}$ is to find in succession two matrices $\boldsymbol{A}$ and $\boldsymbol{B}$ such that

$$\begin{aligned} &1.\ \boldsymbol{A}^{T}\boldsymbol{V}_{\Sigma}\boldsymbol{A}=identity \\ &2.\ \boldsymbol{B}^{T}\left(\boldsymbol{A}^{T}\boldsymbol{V}_{R}\boldsymbol{A}\right)\boldsymbol{B}=diagonal \end{aligned} \qquad (4.1)$$

from which we obtain a matrix satisfying (3.5) as

$$\boldsymbol{F}=\boldsymbol{A}\boldsymbol{B}\,. \qquad (4.2)$$

Matrices $\boldsymbol{A}$ and $\boldsymbol{B}$ are easily found by means of eigenvalue-eigenvector decomposition (EVD) with a two-step procedure. Let $EVD(\boldsymbol{V}_{\Sigma})=\boldsymbol{\Gamma}_{\Sigma}\boldsymbol{\Psi}_{\Sigma}\boldsymbol{\Gamma}_{\Sigma}^{T}$, where $\boldsymbol{\Gamma}_{\Sigma}$ holds in columns the eigenvectors and $\boldsymbol{\Psi}_{\Sigma}$ holds in diagonal the eigenvalues. We set $\boldsymbol{\Psi}_{\Sigma}^{-1/2}\boldsymbol{\Gamma}_{\Sigma}^{T}=\boldsymbol{A}^{T}$ and the first relation of (4.1) is verified. Then, let $EVD(\boldsymbol{A}^{T}\boldsymbol{V}_{\mathrm{L}}\boldsymbol{A})=\boldsymbol{\Gamma}_{\mathrm{L}}\boldsymbol{\Psi}_{\mathrm{L}}\boldsymbol{\Gamma}_{\mathrm{L}}^{T}$. Setting $\boldsymbol{\Gamma}_{\mathrm{L}}^{T}=\boldsymbol{B}^{T}$, (4.1) is verified altogether (Fukunaga, 1990; Schott, 1997).

In section 3 we advanced an analogy between the beamspace and the source space within a BSS framework. Here we make use of this analogy. Particularly, the matrix $\boldsymbol{F}^{T}$ (see section 3) is the equivalent of the *unmixing* matrix. The *mixing* matrix is therefore its pseudo-inverse

$$\boldsymbol{G}=\left(\boldsymbol{F}^{T}\right)^{+}=\left(\boldsymbol{B}^{T}\boldsymbol{A}^{T}\right)^{+}=\boldsymbol{\Gamma}_{\Sigma}\boldsymbol{\Psi}_{\Sigma}^{1/2}\boldsymbol{\Gamma}_{L}\,, \qquad (4.3)$$

where we have been using the orthogonality of eigenvector matrices. Note that $\boldsymbol{G}\neq\boldsymbol{F}$ as a consequence of the fact that the joint diagonalizer is not orthogonal unless $\boldsymbol{V}_{\Sigma}$ and $\boldsymbol{V}_{\mathrm{L}}$ commutes in multiplication (Schoot, 1997, p 155-157), which in general is not the case. Nonetheless, there is a one-to-one relation between the columns of $\boldsymbol{G}$ and the columns of $\boldsymbol{F}$. Figure 4 shows the sLORETA

images corresponding to the first five and last five among the 27 (N-1) non-null columns of $\boldsymbol{G}$, which represent scalp *spatial patterns* of left and right finger movement intention. This is a well-known result routinely employed in the BSS literature. Letting $\boldsymbol{g}_d$ be a column of $\boldsymbol{G}$, with d=1…27, the corresponding sLORETA source power estimation all over the volume is obtained computing $\boldsymbol{g}_d^T \boldsymbol{Q}_\lambda \boldsymbol{g}_d$ at each voxel λ, following (2.8). Since the spatial patterns reflect source activity, which we assume to be noiseless, these sLORETA source power estimations have been here obtained without regularization. Note that obtaining $\boldsymbol{F}$ and $\boldsymbol{G}$ from the joint diagonalization of $\boldsymbol{V}_\Sigma$ and $\boldsymbol{V}_\mathrm{R}$ (instead that of $\boldsymbol{V}_\Sigma$ and $\boldsymbol{V}_\mathrm{L}$) is equivalent, in that the resulting columns of both matrices (hence the spatial patterns) are the same in reverse order, which results from the construction of the filter (3.5). That is why this joint diagonalization method has been called "common spatial pattern", although this terminology may seem contradictory, in that those patterns seek indeed the spatial "uncommonality" between the "left" and "right" covariance structure.

Figure 4 illustrates appropriately the formation of a beamspace, an indecision space and the antibeamspace, according to terminology introduced in section 3. Spatial patterns are arranged in pairs and so are the columns of the filter. The source activity of interest is the desynchronization of the sectors of the primary motor cortex corresponding to the left and right finger movement intention, which in figure 4 is seen as increased source power in the ipsilateral side (see subsection 4.2.). Notice the contralateral correspondence of the first two (left beamspace, or right antibeamspace) and last two (right beamspace, or left antibeamspace) spatial patterns. Spatial patterns from 3 to 25, included, describe the indecision region (among those, only patterns 3-5 and 23-25 are shown). They correspond to vectors with little separation capability since their sources do not belong to regions where a consistent difference in source power for left and right movements is observed. More importantly, the differences observed for those vectors are not localized in the primary motor cortex. Based on this analysis we set D=2 (the beamspace dimension defined in section 3). Therefore the actual filters employed are

$$\boldsymbol{F}_L = \left[\bar{\boldsymbol{f}}_1 \bar{\boldsymbol{f}}_2 \right], \quad \boldsymbol{F}_R = \left[\bar{\boldsymbol{f}}_{27} \bar{\boldsymbol{f}}_{26} \right], \qquad (4.4)$$

where $\bar{\boldsymbol{f}}_d$ is the unit norm d^{th} column of $\boldsymbol{F}$ in (4.2). The normalization fulfils the constraint of the maximization problems stated in (3.4) and assign equal weight to each projection vector.

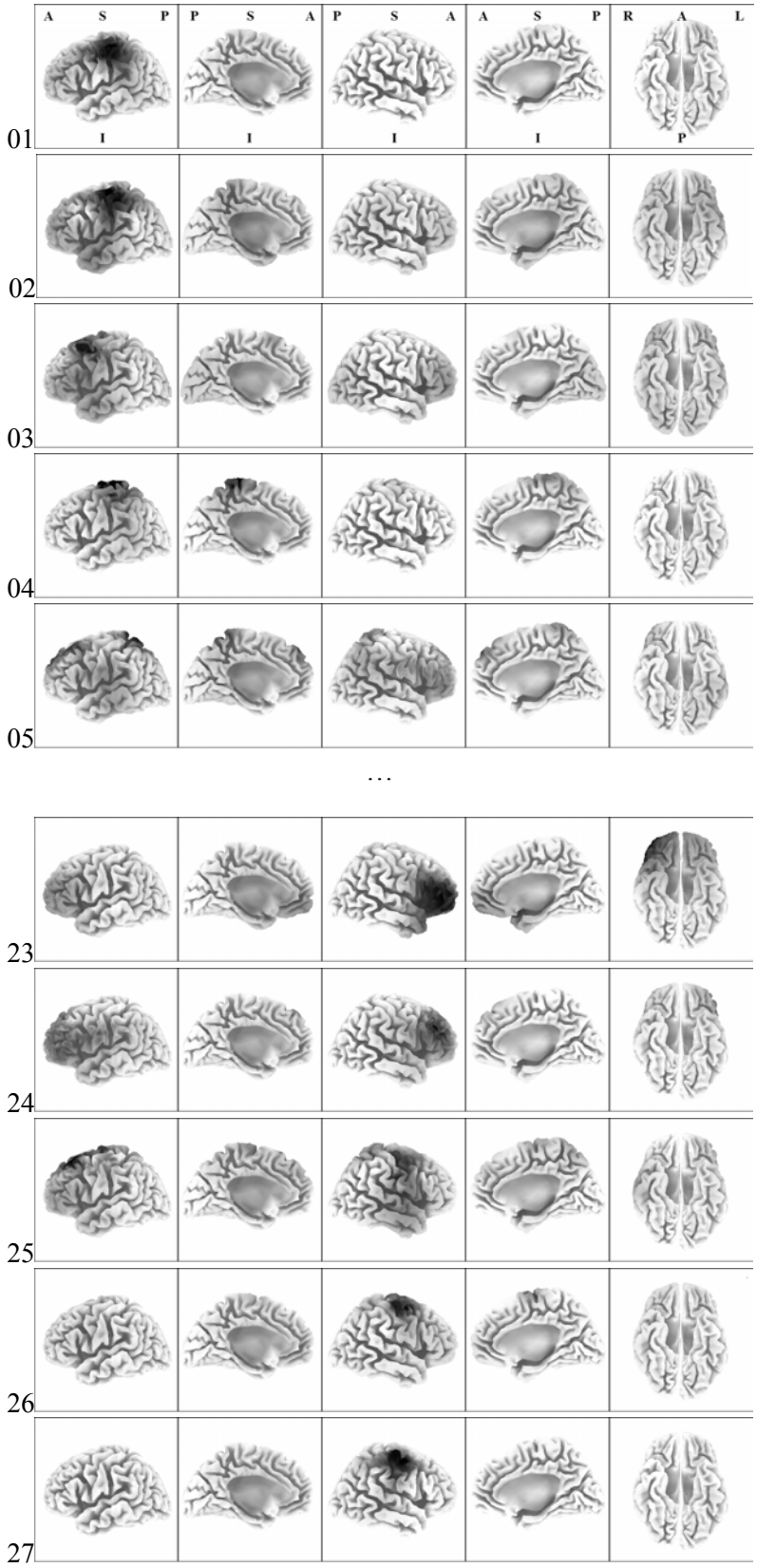

Figure 4. sLORETA cortical images of the spatial patterns associated with vector 1-5 and 23-27 of the spatial filter. The spatial patterns are the vectors of the mixing matrix $\boldsymbol{G}$ as defined in (4.3). For each image, from left to right, are shown the left lateral and medial view, the right lateral and medial view and the bottom view. Each image is scaled to its own maximum. The activity is color-coded with black representing the maximum and white representing zero. Legend: A=Anterior; P=Posterior; S=Superior; I=Inferior; L=Left; R=Right;

4.4. Definition of the Regions of Interest

The next step is the definition of the *location* and *extent* of the two ROIs L and R best differentiating left and right fingers movement intention respectively. For this purpose we use the regularized filtered source power estimation of the grand average sensor measurements outer product matrix for training data corresponding to left and right fingers movement intention. Using (3.3) for each voxel λ, we obtain such a grand average estimation as $tr\left(\boldsymbol{H}_\lambda^T \hat{\boldsymbol{V}}_L \boldsymbol{H}_\lambda\right)$ for left fingers movement intention and $tr\left(\boldsymbol{H}_\lambda^T \hat{\boldsymbol{V}}_R \boldsymbol{H}_\lambda\right)$ for right fingers movement intention. In the above expressions $\boldsymbol{H}_\lambda$ is the $N{\cdot}3$ full-rank factorizations of the inverse quadratic form operator for voxel λ, while $\hat{\boldsymbol{V}}_L = \boldsymbol{F}_L \boldsymbol{F}_L^T \boldsymbol{V}_L \boldsymbol{F}_L \boldsymbol{F}_L^T$ and $\hat{\boldsymbol{V}}_R = \boldsymbol{F}_R \boldsymbol{F}_R^T \boldsymbol{V}_R \boldsymbol{F}_R \boldsymbol{F}_R^T$ are the projected grand average outer product matrices for left and right finger movement intention. Deriving the images from actual EEG data, the regularization helps in suppressing the noise. The resulting sLORETA images are shown in figure 5.

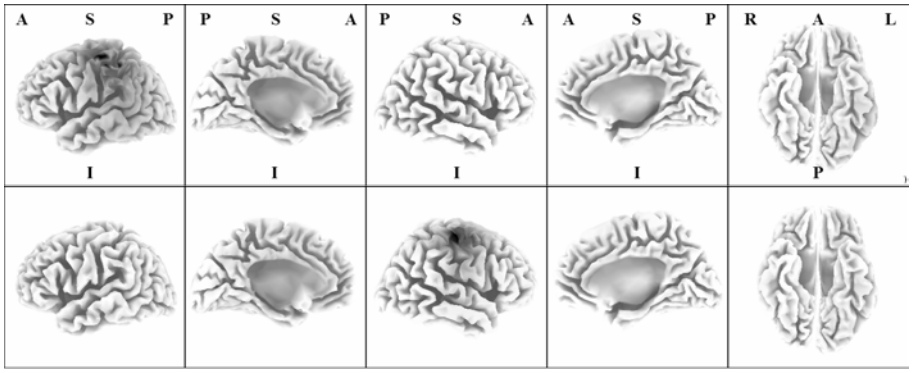

Figure 5. Regularized sLORETA cortical images showing the filtered source power of left (top row) and right (bottom row) finger movement intention grand average training trials. For the meaning of the graphical representation and legend see the caption of figure 4.

Figure 5 shows that the filtered average source power has high spatial specificity for the two involved sectors of the primary motor cortex. The two activation regions are nearly symmetric along the midline. The region on the left hemisphere has maximum (2.91e-7) at Talairach coordinates x=-59, y=-39, z=50, while the region on the right hemisphere has maximum (1.47e-7) at x=53, y=-18, z=57. As compared to the right region, the maximum of the left region is located 6 mm more lateral (x-axis), 21 mm more posterior (y-axis) and 7 mm more inferior (z-axis). The only relevant asymmetry seems to be along the y-axis. There are many reasons that could account for this, including 1) asymmetry of the motor cortex in this individual, 2) the use of a spherical head model, 3) asymmetry of electrode placements, 4) noise, and 5) the non homogeneous scalp sampling due to the electrode placement for this experiment (Michael *et al*, 2004; Van Veen *et al*, 1997), which is shown in figure 1. It is noteworthy that the first of the above causes of concern is not critical for our purpose, because the head anatomy is constant. On the other hand the last four may have affected the accuracy of the source localization and may limit the classification accuracy based on source localization. In any case, the agreement of these images with the results of the permutation test (figure 2) is substantial.

The motor cortex has a topographic organization and body parts follow closely in their cortical representation. Therefore we assume that the sources implicated with finger movement have small coverage. Our current space sampling allows a resolution of 7mm^3. We estimated the voxel carrying maximal divergence (as seen on data by the spatial filter) to be a good representation of the neuronal activity of interest. Thus we define the left ROI L and right ROI R as the voxels displaying the maxima in figure 5. This choice was also suggested by the performance of a simple linear classifier (on the training set) obtained using ROIs centered at the maxima and varying their dimension.

4.5. Classification of the Test Set

Classifying trials in which membership is unknown requires a classification *criterion*. Traditionally BCI relies on trained classifiers; a learning algorithm is employed and its job is to learn how to assign membership based on training data. In the introduction we stated that our approach is hybrid. We do not rely on iterative ICA algorithms to extract the activity of interest from each trial. Rather, we use training data to design a filter able to accomplish the same task, but much faster. The other advantage of our approach is that the classification algorithm itself is untrained. Given a test trial with average sensor measurements outer product $\boldsymbol{V}_{test}$ we obtain directly the filtered source power estimation in L as (see equation (3.6))

$$\hat{\gamma}_L = tr\left(\boldsymbol{H}_L^T \boldsymbol{F}_L \boldsymbol{F}_L^T \boldsymbol{V}_{test} \boldsymbol{F}_L \boldsymbol{F}_L^T \boldsymbol{H}_L\right) \qquad (4.5)$$

and in R as

$$\hat{\gamma}_R = tr\left(\boldsymbol{H}_R^T \boldsymbol{F}_R \boldsymbol{F}_R^T \boldsymbol{V}_{test} \boldsymbol{F}_R \boldsymbol{F}_R^T \boldsymbol{H}_R\right). \qquad (4.6)$$

The classification criterion is then simply set such as

$$\begin{cases} \text{classify trial as } \textit{left} \text{ finger movement intention if } \hat{\gamma}_L > \hat{\gamma}_R \\ \text{classify trial as } \textit{right} \text{ finger movement intention if } \hat{\gamma}_L < \hat{\gamma}_R \end{cases}, \qquad (4.7)$$

that is, after plotting in a Cartesian space the point with coordinates $\left(\hat{\gamma}_L,\ \hat{\gamma}_R\right)$, the classifier is the line with equation $y=x$.

It has been found that movement-related potentials associated to different body parts do not differ on the scalp as soon as the movement is planned. Rather, in a first phase, starting several seconds before electromyographic (EMG) activity, the potentials are indistinguishable. In a second phase, starting approximately 500 ms before EMG onset, the potential associated to different body parts begin to diverge. This divergence is more pronounced on the vertex (Cz electrode) and increase as the EMG onset approaches, being maximal just before EMG onset (Jankelowitz and Colebatch, 2002). Thus, it appears that the preparatory phase engender common spatial activation, whereas body part-specific activity takes place shortly before the actual movement. Our classification method relies on the spatial segregation of brain activity related to the intention of movement of different body parts. Based on these evidences, the test trial average outer product matrix as computed only the last portion of the trial may carry more spatial specific information that the average outer product matrix computed on the whole available trial. For each test trial we repeated the classification task using $\boldsymbol{V}_{test}$ computed on the whole available data (500 ms for this benchmark) and using $\boldsymbol{V}_{test}$ computed on the last 250 ms only.

The pre-processing steps to which the test data was submitted were exactly the same to which the training data were submitted. Namely, the trials were down-sampled to 128 samples per second and band-pass filtered in the region 14-26 Hz. The classification processing consisted uniquely in source power magnitude comparison as per (4.7).

4.6. Results

The accuracy rate in this study is defined as the proportion of correctly classified test trials. This was the accuracy criterion used in the BCI competition 2003. The data set contains a total of 100 test trials, of which 49 pertain to left finger movement intention and 51 to right finger movement intention. Plots of filtered source power estimation in L and R for both left and right fingers movement intention, for the training and test set and estimating the average outer product matrix from all available 500 ms or only the last 250 ms, are shown in figure 6 (A, B, C, D). As a comparison, plots of unfiltered source power in the same ROIs (raw sLORETA) obtained considering the last 250 ms for each trial are shown in Fig 6 (E, F). Those may be directly compared to figure 6 (C, D). For graphical accommodation, we plot the natural logarithm of the source power estimation previously multiplied by a large constant (10^5). Using only the last 250 ms the classification accuracy for the training set (figure 6D) equals 83% using the filter, which is very close to the score reached by the winners of the competition for this data set (84%: Wang *et al*, 2004), despite our use of an untrained classifier and only one attribute for each class was extracted. On the other hand the classification accuracy employing sLORETA without spatial filtering on the

same data is significantly lower (78%: figure 6F). It should be noted that when using no spatial filter the points are more scattered, indicating lower classification power.

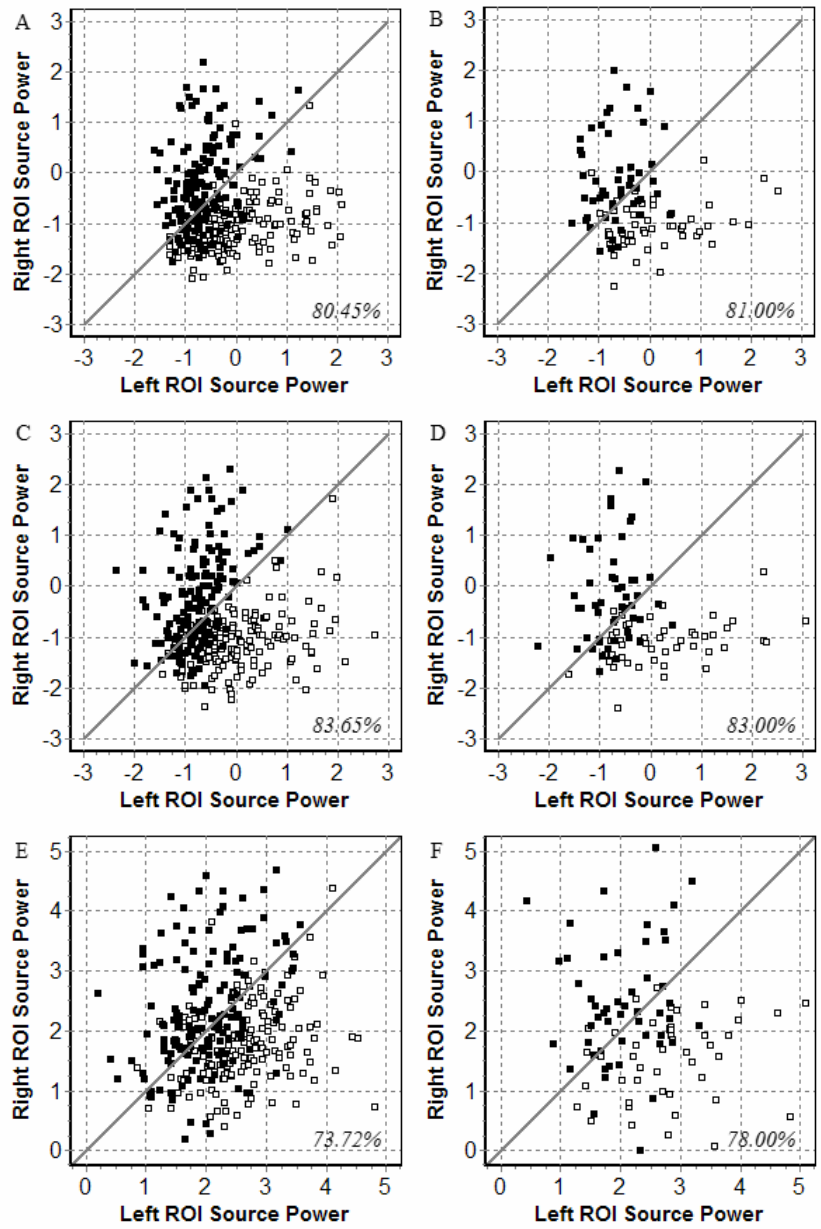

Figure 6. Scatter plots depicting the results of the classification. In each plot on the x-axis and y-axis is the source power in the left and right region of interest (ROI), respectively. Left column (A, C, E): results on the training set (159 Left + 157 Right trials). Right column (B, D, F): results on the test set (49 Left + 51 Right trials) . Top row (A, B): results obtained using the filter on the whole available 500 ms for each trial. Middle row (C, D): results obtained using the filter on the last 250 ms for each trial. Bottom row (E, F): results obtained with no filter (raw sLORETA) on the last 250 ms for each trial. The untrained classifier is represented by the thick grey line, which has equation $y=x$. According to (4.7), right fingers movement intention trials (black squares) are correctly classified if they fall above the line, while left fingers movement intention trials (white squares) are correctly classified if they fall below the line. The classification accuracy is printed as percentage of correctly classified trials near the bottom-right corner of each plot.

5. Conclusions and Discussion

The aim of this paper was to investigate the coupling of sLORETA and a data-driven filter for the purpose of classifying movement-related desynchronization engendered by finger movement intention. The filter here adopted may be conceived as a beamformer particularly designed for classification purposes and its application to an EEG inverse solution has been proposed here for the first time. As shown, a source localization method alone does not allow sufficient classification power for the purpose of classifying motor cortex desynchronization. For this reason previous works relied on either independent component analysis or on a trained classifier. In actual BCI implementations the first approach (Jun *et al*, 2005; Qin *et al*, 2004) would require dedicated parallel processing units in order to extract the independent component in real-time. Furthermore, the automatic selection of relevant independent components is cumbersome. The second (Grave de Peralta Menendez *et al*, 2005) would require a long training phase for the classifier, still, it is our impression that any attempt to use raw inverse solutions to localize movement-related desynchronizations from the noisy single-trial EEG is vain. Our approach has been presented as hybrid, in that on one hand a learning phase is required to estimate the spatial filter and on the other the classifier is untrained. The advantage of such an approach is the speed of computations required (matrices $\boldsymbol{F}_{\mathrm{L}}\boldsymbol{F}_{\mathrm{L}}{}^{T}\boldsymbol{H}_{\mathrm{L}}$ in (4.5) and $\boldsymbol{F}_{\mathrm{R}}\boldsymbol{F}_{\mathrm{R}}{}^{T}\boldsymbol{H}_{\mathrm{R}}$ in (4.6) are computed off-line) preserving the ability to adapt to the individual brain characteristics. No automatic selection of independent component is required. Therefore our approach is suitable for actual BCI applications as it stands.

Since the spatial filter is data-driven, new available trials can be used to refine the projection filters $\boldsymbol{F}_{\mathrm{L}}\boldsymbol{F}_{\mathrm{L}}{}^{T}$ and $\boldsymbol{F}_{\mathrm{R}}\boldsymbol{F}_{\mathrm{R}}{}^{T}$ on the background while the BCI system is at work. Given that only prototypical trials are used to update the filter, we may expect the spatial filter so constructed to be asymptotically optimal. The method presented hereby reached 83% classification accuracy on the test set using the last 250 ms of data for each trial. The result is obtained using a single feature. An inspection of the scatter plots in the right column of figure 6 reveals that some of the misclassified test trials are far away from the separating line. This is especially true for right finger movement intention trials (black squares in the figure). These data suggest that the obtained classification accuracy could not be dramatically improved over the current result using only the event-related desynchronization feature. Many research teams analyzed this data set for the BCI competition 2003 using a great variety of features and classification algorithms, yet only Wang *et al* (2004) outperformed the present result. Hence, we may actually hypothesize that the obtained classification accuracy could not be dramatically improved upon, even using additional features and trained classifiers. Rather, for some trials the membership may be confounded. This is a natural occurrence in an experiment involving self-paced repetitive tasks in which the subject may not be able to keep a constant level of concentration and performance throughout the duration of the experiment.

It may be surprising that using an untrained classifier and a single feature, we obtain nearly the same classification accuracy obtained by Wang *et al* (2004), who used a trained classifier and three features, two related to the Bereitschaft potentials and one related to the event-related desynchronizations. Two common mistakes in classification tasks amount to improper definition of attributes and to the assumption that the best classifier is the one best fitting the training set. Multiple attributes are useful as long as their joint probability vanishes. It is well-known that if this is not the case, multiple attributes are redundant and the SNR drops down. On the other hand, one should not seek necessarily the best fit of the training data, since such a classifier guarantees fitting of the available sample, but not of the population of interest. This phenomenon is knows as *overlearning*. Actually, the smaller the number of observations (training trials) and the lower their SNR, the lower the ability to estimate the best classifier from that sample. Rather, one should seek, as much as possible, parameters independent from the training data to tune the classifier. This is the strategy we followed. Wang *et al* (2004) reported 92.98% classification accuracy on the training set and 84% on the test set. Such a difference is a typical outcome of overlearning. Our classifier features similar classification accuracy for the training and test set, both using 500 ms of data or only the last 250 ms (figure 6). This shows that our classifier did not overlearn (actually it did not learn at all). Sure enough we could have marginally increased the classification accuracy of this data set adding a feature related to the Bereitschaft potentials. However, our aim was restricted at

showing the feasibility of classifying movement-related desynchronizations by coupling an accurate inverse solution with a suitable data-driven spatial filter.

In EEG, the SNR of single-trials is very low and the noise affects the localization accuracy of linear inverse solutions. The data-driven filter we designed aims at separating the interesting components associated to the movement intention. In doing so it clearly has a noise-suppression capability. However, we cannot ascertain at the present stage if the previous use of blind source separation would provide additional advantages for noise removal.

The method currently presented is subject to major improvements, especially related to the definition of the *location* and *extent* of the brain regions of interest involved in motor planning. It should be stressed here that spatial segregation of sources belonging to different classes does not assume that the sources are point-like or that they are confined to small neuronal populations. As long as the sources are spatially segregated, the linear superposition principle holds and sources may as well be composed of clusters of neuronal populations, physiologically connected, but possibly far away from each other in space (Van Veen *et al*, 1997). The accurate definition of such neuronal grouping is therefore a major task for the success of the method and a challenging line of research for future investigations. In addition, multiple regions may be employed, associated to multiple frequency and temporal windows. Of course, the use of a more realistic head model based on the magnetic resonance images of the subject and the use of more electrodes would increase the accuracy of the source localization method itself, hence of the method described in this paper altogether. Further margin for improvement concerns the definition of the prototypical covariance structures $\boldsymbol{V}_{\mathrm{L}}$ and $\boldsymbol{V}_{\mathrm{R}}$ used to define the filter (Section 3). In this respect ICA may be very useful.

There are several indicators that suggest movement-related brain activity has a distinct spatio-temporal course. Early motor planning seems to be generated in the supplementary motor area (SMA), whereas other pre-motor areas seem to be involved before the primary motor cortex itself (Jankelowitz and Colebatch, 2002). Implication of the SMA in this study is noticeable in the pair of spatial patterns 3 and 25 (figure 4). Detection of SMA activation may prove useful for early detection of movement intention, a fundamental task necessary for actual BCI applications. The time course of brain activations, specific in space and frequency, may constitute a powerful way to exploit the advantage of EEG inverse solution over raw scalp potentials. For this reason we believe that source localization methods are going to draw more and more attention in the BCI community.

Acknowledgments

This Research has been partially funded by the French National Research Agency (ANR) within the National Network for Software Technologies (RNTL), project Open-ViBE (Open Platform for Brain Environments), and by Nova Tech EEG, Inc., Knoxville, TN. The authors wish to express their gratitude to Dr. Bernard Hennion, Dr. Noland White and Dr. Leslie Sherlin for the helpful comments on a preliminary draft of this paper. They also would like to thank an anonymous reviewer for his comments on equation (3.6).

Appendix

We here remind a classic result of linear algebra proving the last equality in equation (2.1). We are concerned with quadratic forms of the kind $\boldsymbol{v}^T(t)\boldsymbol{Q}\boldsymbol{v}(t)$, with $\boldsymbol{v}(t)$ non-null and $\boldsymbol{Q}$ positive-definite, symmetric and non defective. In the following we omit the time index. Let $P=rank(\boldsymbol{Q})$. Then, the eigenvalue-eigenvector decomposition

$$\boldsymbol{Q} = \boldsymbol{U}\boldsymbol{w}\boldsymbol{U}^T = \begin{bmatrix} \boldsymbol{U}_\mu & \boldsymbol{U}_\eta \end{bmatrix} \begin{bmatrix} \boldsymbol{W}_\mu & \boldsymbol{0} \\ \boldsymbol{0} & \boldsymbol{0}_\eta \end{bmatrix} \begin{bmatrix} \boldsymbol{U}_\mu & \boldsymbol{U}_\eta \end{bmatrix}^T$$

is such that $\boldsymbol{U}_\mu$ contains, in columns, the P dominant eigenvectors and $\boldsymbol{U}_\eta$ contains the remaining N-P eigenvectors; similarly, $\boldsymbol{W}_\mu$ holds, in diagonal, the P positive eigenvalues, with $W_1 \geq \ldots \geq W_P > (W_{P+1} \ldots W_N = 0)$. If we pose $P \cdot N$ matrix $\boldsymbol{H}^T = \boldsymbol{W}_\mu^{1/2}\boldsymbol{U}_\mu^T$ such that $\boldsymbol{H}\boldsymbol{H}^T = \boldsymbol{Q}$ and project the sensor measurements space into $\boldsymbol{z}=\boldsymbol{H}^T\boldsymbol{v}$, it follows $\boldsymbol{v}^T\boldsymbol{Q}\,\boldsymbol{v} = \sum_{p=1}^{P} z_p^2$. The equality is seen as $\sum_{p=1}^{P} z_p^2 = \boldsymbol{z}^T\boldsymbol{z} = \boldsymbol{v}^T\left(\boldsymbol{U}\boldsymbol{W}^{1/2}\boldsymbol{W}^{1/2}\boldsymbol{U}^T\right)_\mu \boldsymbol{v} = \boldsymbol{v}^T\boldsymbol{Q}\,\boldsymbol{v}$.

References

Backus G and Gilbert F 1968 The resolving power of gross earth data *Geophys J R Asr Soc* **16**, 169-205

Blanchard G and Blankertz B 2004 BCI Competition 2003—Data set IIa: Spatial Patterns of Self-Controlled Brain Rhythm Modulations *IEEE Trans. on Biom. Img.* **51**(6) 1062-1066

Blankertz B, Curio G and Müller K R Classifiyng Single Trial EEG: Toward Brain Computer Interfacing, In T G Diettrich, S Becker and Z Ghahramani (Ed) 2002 Advances in Neural Information Processing Systems (NIPS 01) **14** 157-164

Blankertz B, Müller K R, Curio G, Vaughan T M, Schalk G, Wolpaw J R, Schlgl A, Neuper C, Pfurtscheller G, Hinterberger T, Schrder, M and Birbaumer N 2004 The BCI Competition 2003: Progress and Perspectives in Detection and Discrimination of EEG Single Trials *IEEE Trans. on Biom. Eng.* **51**(6) 1044-1051

Bolton J P, Gross J, Liu L C and Ioannides A A SOFIA: spatially optimal fast initial analysis of biomagnetic signals 1999 *Phys. Med. Biol.* **44** (1) 87-103

Cichocki A and Amari S I 2002 *Adaptive Blind Signal and Image Processing Learning Algorithms and Applications* John Wiley & Sons, New-York

Congedo M, Ozen C and Sherlin L 2002 Notes on EEG Resampling by Natural Cubic Spline Interpolation *J. Neuroth.* **6**(4) 73-80

Fukunaga K 1990 *Introduction to Statistical Pattern Recognition* (2nd Ed) Academic Press, New York

Grave de Peralta Menendez R, González Andino S, Perez L, Ferrez P W and Millán J del R 2005 Non-invasive estimation of local field potentials for neuroprosthesis control, *Cogn. Proc.* **6** 59-64

Greenblatt R E, Ossadtchi A and Pflieger M E 2005 Local Linear Estimators for the Bioelectromagnetic Inverse Problem *IEEE Trans. Sig. Proc.* **53** (9) 3403 - 3412

Gross J and Ioannides A A 1999 Linear Transformation of data space in MEG *Phys. Med. Biol.* **44**(1) 87-103

Guger C, Ramoser H and Pfurtscheller G 2000 Real-Time EEG Analysis with Subject-Specific Spatial Patterns for a Brain-Computer Interface, *IEEE Trans. Reh. Eng.* **8(**4) 447-456

Hyvärinen A, Karhunen J and Oja E 2001 *Independent Component Analysis* John Wiley & Sons, New York

Holmes A P, Blair R C, Watson J D G and Ford L 1996 Nonparametric Analysis of Statistic images from functional mapping experiments, *J. Cereb. Blood Flow Metab.* **16** 7-22

Jankelowitz S K and Colbatch J G 2002 Movement-Related Potentials Associated with Self-Paced, Cued and Imagined Movements *Exp.Brain Res.* **147**, 98-107

Jun S C and Pearlmutter B A 2005 Fast Robust Subject-Independent Magnetoencephalographyc Source Localization using an Artificial Neuronal Network *Human Brain Map.* **24** 21-34

Koles Z J 1991 The Quantitative extraction and Topographic Mapping of the Abnormal Components in the Clinical EEG *Electroenc. Clin. Neuroph.* **79** 440-447

Koles Z J and Soong A 1998 EEG Source Localization: Implementing the Spatio-Temporal Decomposition Approach *Electroenc. Clin. Neuroph.* **107** 343-352

Kübler A, Kotchoubey B, Kaiser J, Wolpaw J R and Birbaumer N 2001 Brain-computer communication: unlocking the locked in *Psychol Bull*, **127(**3) 358-75

Lopes da Silva F 2004 Functional Localization of Brain Sources using EEG and/or MEG data: Volume Conductor and Source Models *Magn. Res. Img.* **22** 1533-1538

Lubar J F, Congedo M and Askew J H 2003 Low-resolution electromagnetic tomography (LORETA) of cerebral Activity in chronic depressive disorder *Int. J. Psychoph.* **49(**3) 175-185

Michel C M, Murray M M, Lantz G, Gonzalez S, Spinelli L and Grave de Peralta Menendez R 2004 EEG Source Imaging *Clin. Neurophy.* **115** 2195-2222

Müller K R, Krauledat M, Dornhege G, Curio G and Blankertz B 2004 Machine learning techniques for brain-computer interfaces, *Biomed. Tech.* **49** 11–22

Neumann N, Kübler A, Kaiser J, Hinterberger T and Birbaumer N 2003 Conscious Perception of Brain States: Mental Strategies for Brain-Computer Communication, *Neuropsychologia,* **41** 1028-1036

Parra L and Sajda P 2003 Blind Source Separation via Generalized Eigenvalue Decomposition *J. Mach. Learn. Res.* **4** 1261-1269

Pascual-Marqui R D 1999a Review of Methods for Solving the EEG Inverse Problem *Int. J. Bioelectrom.* **1(**1) 75-86

Pascual-Marqui R D 1999b Reply to Comments made by R Grave de Peralta Menendez and SI: Gonzalez Andino *Int. J. Bioelectrom.* **1(**2)

Pascual-Marqui R D 2002 Standardized Low-Resolution Brain Electromagnetic Tomography (sLORETA): technical details *Meth. Find. in Exp. Clin. Pharmac.* **24D** 5-12

Pfurtscheller G, Flotzinger D and Kalcher J 1993 Brain-computer interface-a new communication device for handicapped persons, *J. Microcomp. Applic.* **16** 293–299

Qin L, Ding L and He B 2004 Motor Imagery Classification by Means of Source Analysis for Brain-Computer Interface Applications *J. Neural Eng.* **1** 135-141

Ramoser H, Muller-Gerking J and Pfurtscheller G 2000 Optimal Spatial Filtering of single trial EEG during Imagined Hand Movement *IEEE Trans. on Reh. Eng.* **8(**4) 441-446

Rodríguez-Rivera A, Baryshnikov B V, Van Veen B D, Wakai R T 2006 MEG and EEG Source Localization in Beamspace, *IEEE Trans. Biom. Eng.*, **53**(3), 430-441.

Sarvas J 1987 Basic Mathematical and Electromagnetic Concepts of the Biomagnetic Inverse Problem, *Phys. Med. Biol.* **32(**1)11-22

Schott J R 1997 *Matrix Analysis for Statistics* John Wiley & Sons, New-York

Sekihara K, Sahani M and Nagarajan S S 2005 Localization Bias and Spatial Resolution of Adaptive and non-Adaptive Spatial Filters for MEG Source Reconstruction *Neuroimage* **25(**4) 1056-67

Talairach J and Tournoux P 1988 *Co-planar stereotaxic atlas of the Human Brain*, Thieme, New York

Van Veen B D and Buckley M 1988 Beamforming: A Versatile Approach to Spatial Filtering *IEEE ASSP Mag.* **5** 4-24

Van Veen B D, van Drongelen W and Suzuki A 1997 Localization of Brain Electrical Activity via Linearly Constrained Minimum Variance Spatial Filter *IEEE Trans. Biom. Eng.* **44(**9) 867-880

Wang Y, Zhang Z, Li Y, Gao X and Gao S 2004 BCI Competition 2003-Data set IV: an Algorithm Based on CSSD and FDA for classifying Single-Trial EEG *IEEE Trans. on Reh. Eng.* **51(**6) 1081-1086

Westfall P H and Young S S 1993 *Resampling-Based Multiple Testing Examples and Methods for p-Values Adjustment* John Wiley & Sons, New York

Wolpaw J R, Birbaumer N, McFarland D J, Pfurtscheller G and Vaughan T M 2002 Brain Computer Interface for communication and control *Clin. Neurophy.* **113** 767-791